PCCP

Lattice–gas study of the kinetics of the NO–CO catalytic reaction on Pd nanoclusters

V. Bustos,[a] R. O. Uñac,[a] G. Zgrablich*[b] and Claude R. Henry[c]

[a] *Laboratorio de Ciencias de Superficies, Universidad Nacional de San Luis, Chacabuco, 917, 5700, San Luis, Argentina*
[b] *Departamento de Química, Universidad Autónoma Metropolitana, Iztapalapa, P.O. Box 55-534, México D.F. 09340, México;. E-mail: giorgiozgrablich942@hotmail.com*
[c] *CRMC2-CNRS, Campus de Luminy, case 913, 13288, Marseille cedex 09, France*

Received 11th March 2003, Accepted 9th May 2003
First published as an Advance Article on the web 29th May 2003

The kinetics of the NO–CO reaction on Pd nanoclusters is studied through a lattice–gas model and Monte Carlo simulation. Pd nanoclusters with three typical sizes: 2.8 nm, 6.9 nm and 15.6 nm, are considered. These nanoclusters have been epitaxially grown on MgO(100) and tested for the NO–CO reaction in previous experimental work [ref. 9–11: C. H. F. Peden, D. W. Goodman, D. S. Blair, P. J. Berlowitz, G. B. Fisher and S. H. Oh, *J. Phys. Chem.*, 1988, 92, 1563; C. Duriez, C. R. Henry and C. Chapon, *Surf. Sci.*, 1991, 253, 190; L. Piccolo and C. R. Henry, *Appl. Surf. Sci.*, 2000, 162–163, 670], thus providing the motivation for the present study. According to their size, the nanoclusters present different proportions of Pd(100) and Pd(111) facets. The effects of CO and NO desorption are found to be of fundamental importance for the behavior of the system. In all cases the medium size particles are found to be the most active. At low temperature, where NO desorption can be neglected (since the activation energy for desorption of NO on Pd is about 5 kcal mol^{-1} greater than that for the desorption of CO), the largest particles are revealed as the less active, while at high temperature, where both NO and CO desorption take place, the smallest particles are found to be the less active. These results are in concordance with the experimentally observed behavior.

1. Introduction

The catalytic reduction of NO by CO on metals is of great importance in the problem of air pollution control, and as such it has received the continuous attention of both experimentalists and theoreticians for many years.[1–21] It is well known[16,18,21] that this is a particular case of a monomer–dimer reaction which can be sustained in the steady state regime only within a range of the gas phase composition, in this range it is said that we have a reaction window. Outside the reaction window the reaction dies out as the metal surface becomes poisoned, *i.e.*, covered by one or more species which are no longer able to react. In the case of NO–CO reaction, this reaction window is the manifestation of a bi-stability induced by a delicate site–particle stoichiometric balance: the monomer (CO) needs one single site to adsorb, while the dimer (NO), even if it can adsorb initially on a single site, needs an additional nearest-neighbor (NN) vacant site in order to dissociate and allow for the reaction to continue. Therefore the study of the kinetics of the reaction in steady state conditions requires both the determination of the reaction window and the reaction rate within the window.

The majority of previous studies on this catalytic reaction have focused mainly either on ideal systems, that means the reaction is studied on a monocrystal metal face in ultra-high-vacuum conditions, or on real catalytic systems, *i.e.* the catalyst consists of supported metal particles on a porous solid and the experiments are performed at high pressure. The supported particle size and morphology in a real catalyst is not sharply controlled. As a mean to fill the gap between the two extreme kinds of systems, studies should be performed on systems where supported metal particles with controlled size and morphology are used and still the reaction can be followed in a "clean" environment.

Experiments[10–12] have been able to produce palladium clusters grown epitaxially on MgO(100). The size and shape of the Pd nanoparticles were characterized through TEM and their behavior in the NO reduction by CO was determined by means of molecular beam techniques. Three samples of the model catalyst contained Pd particles with size distributions around typical sizes of 2.8 nm, 6.9 nm and 15.6 nm; they contained a proportion of (100)/[(100) + (111)] facets of approximately 0.20, 0.25 and 0.75, respectively. Effective turnover rates for different products of the reaction were found to depend on the particle size in such a way that the intermediate size was the most active at all temperatures. It was also found that the largest particles are the less active at low temperature, while the smallest particles are the less active at high temperature.[12]

These experiments provide a strong motivation to extend the theoretical research of the kinetics of the NO–CO reaction, usually referring to a monocrystal face where boundary effects are reduced by the use of periodical boundary conditions, to the case of nanoparticles presenting different facets and finite size boundary effects. These studies usually rely upon lattice–gas modeling of the system and numerical simulation of the reaction process.

Accordingly, the purpose of the present work is to study the approach of such a reactive system to the steady state regime by means of Monte Carlo simulation. In particular we want to determine the behavior of the reaction window and, within it, the behavior of the reaction rate, as a function of the size and shape of catalytic nanoparticles, and find out to what extent the model predictions are consistent with experimental results.

 DOI: 10.1039/b302778c

In Section 2 we develop the modeling of the system and the simulation method. Results are presented and discussed in Section 3, while Section 4 is dedicated to the comparison with experiments. Finally, general conclusions are given in Section 5.

2. System modeling and simulation method

An active Pd particle is modeled as a truncated pyramid, as summarized in Fig. 1, with a square lattice representing the top face, corresponding to the (100) facet, and triangular lattices representing the four lateral faces, corresponding to the (111) facets. The size of a particle is characterized by its side length, L, in (111) lattice units taken as 0.275 nm for Pd. The proportion of (100) and (111) facets can be changed in order to mimic the morphology of the real Pd particles, used in the experiments, for different sizes.

This kind of structure presents a combination of a higher coordinated surface, the (111) crystal plane, and a lower coordinated one, the (100) crystal plane. From a purely geometric point of view, a higher coordinated surface facilitates both NO dissociation and also the encounter of any two reacting species, it should then be more active than a lower coordinated one. However, experimental studies supported by theoretical calculations[22,23] seem to show that the dissociation increases when the coordination of the surface atoms decreases, but at the same time the bonding of adsorbed N increases and, when the strength of this bond is too high, adsorbed N acts as a poison for the reaction. In conclusion, several arguments are in favor of a greater activity in the CO–NO reaction for the (111) face compared to the (100) face. Moreover, we will also have a certain amount of sites at step edges between facets. These sites may provide stronger bonds for some adsorbed species. Some experimental results[23,24] suggest that NO dissociation leads to two kinds of adsorbed N, a weakly bound and a strongly bound one. Step edge sites in our particles are good candidates to allocate strongly bound N and we wish to explore here the effects of these sites on the reaction. This is done in our model by introducing an inhibition parameter, I, such that whenever a N atom is adsorbed on an edge site the corresponding reaction does not always occur but it does so with a probability $0 \leq I \leq 1$.

As it is well known,[16] Monte Carlo simulations of the NO–CO reaction on (100) or (111) lattices do not present a reaction window unless desorption of NO and/or CO species is assumed. Therefore we introduce the possibility that adsorbed NO and CO can be desorbed with probability D_{NO} and D_{CO}, respectively, while neglecting desorption of any other species. This is a reasonable assumption given that molecularly adsorbed NO and CO are the most weakly adsorbed species among those participating in the reaction, with activation energy for desorption around 30 kcal mol^{-1} for Pd, the activation energy for the desorption of NO being about 5 kcal mol^{-1} higher than that for CO.[12] Taking into account this circumstance, we may expect different behaviors at low and high temperatures, dictated by the fact that at low temperature NO desorption will be negligible compared to CO desorption, while at high temperature both processes are active.

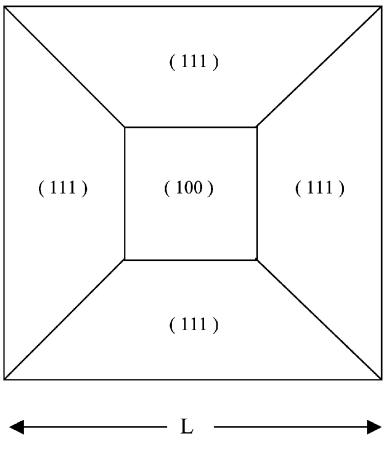

Fig. 1 Lattice model for a Pd nanoparticle epitaxially grown on MgO(100).

Other processes that may affect the reaction are NO and CO surface diffusion, whose activation energy is much lower than that corresponding to the desorption of these species. However, by taking into account desorption, this already in some sense also includes taking into account diffusion,[16] so that we will not consider diffusion processes here.

Finally, the NO dissociation process, the reaction-controlling step, must be specified. It is by now well established that NO adsorbs molecularly on a single site and afterwards it may dissociate, with a given probability P upon the availability of an additional NN vacant site. We follow here a process similar to that used in ref. 16. At adsorption of an NO molecule we test all NN sites for a vacant one, if it is available then NO is dissociated with probability P. Furthermore, whenever a new vacant site is produced, as a consequence of some reaction or desorption step, its NN sites are tested for an NO to dissociate with probability P. This dissociation probability is usually taken as $P = 1$ in the literature. However, experimental evidence from ref. 12 shows that in the studied system NO dissociation efficiency varies from about 0.5 at low temperature (180 °C), where the dissociation is inhibited due to the high surface coverage, to about 0.7 at high temperature (430 °C), where dissociation is much less depressed by the lack of vacant sites. More precisely, the temperature behavior of the dissociation efficiency, see Fig. 8 in ref. 12, is found to be dependent on the Pd particle size: for the smallest and intermediate size particles, of 2.8 and 6.9 nm, it rises rapidly from 0.5 to almost 0.7, while for the largest particle size, of 15.6 nm, it appears to be nearly constant around 0.5 from 180 °C to about 350 °C and then raises rapidly to 0.7. Therefore, it is reasonable to assume that at least a small fraction of adsorbed NO will not dissociate upon the availability of NN vacant sites and we take P as a parameter and study its effects on the reaction kinetics. We take first the value of $P = 0.7$, which seems to be the most reasonable for all cases, and then study the effects of changing its value to extreme values like 0.9 and 0.5.

A collection of active particles of a given size is exposed to a gas phase which is a mixture of NO and CO with molar fractions Y_{NO} and Y_{CO}, respectively, such that they sum up to 1. The system undergoes adsorption, desorption and reaction processes, which can be separated into the following reaction steps:

$$CO(gas) + site \rightarrow CO(ads) \quad (1)$$

$$NO(gas) + site \rightarrow NO(ads) \quad (2)$$

$$NO(ads) + site \xrightarrow{P} N(ads) + O(ads) \quad (3)$$

$$N(ads) + N(ads) \rightarrow N_2(gas) + 2\ sites \quad (4)$$

$$NO(ads) + N(ads) \rightarrow N_2(gas) + O(ads) + site \quad (5)$$

$$NO(ads) + N(ads) \rightarrow N_2O(gas) + 2\ sites \quad (6)$$

$$CO(ads) + O(ads) \rightarrow CO_2(gas) + 2\ sites \quad (7)$$

$$NO(ads) \xrightarrow{D_{NO}} NO(gas) + site \quad (8)$$

$$CO(ads) \xrightarrow{D_{CO}} CO(gas) + site \quad (9)$$

Given that the experimental results obtained in ref. 12 report only a small fraction of the production of N_2O with respect to N_2 (less than 10%), we have fixed the relative rates of steps (5) and (6) to 87% and 13%, respectively. However, this is by

far a secondary matter since a change in these proportions does not affect the general behavior of the system.

We want to study the steady-state regime for the above reaction scheme through Monte Carlo simulation. This is done according to the following procedure: A Monte Carlo trial begins by choosing a molecule from the gas phase with probabilities given by Y_{CO} and $Y_{NO} = 1 - Y_{CO}$.

(i) *If the chosen molecule is NO*, then: (a) choose a site at random on the lattice; (b) if the site is occupied by CO, NO, N or O, then the trial ends; (c) if the site is empty NO is adsorbed and, (c1) its nearest-neighbor sites are checked randomly for an N, if one is not found the trial jumps to (c2), otherwise reaction steps (5) and (6) are executed with probability 0.87 and 0.13, respectively, in case step (6) is executed the O(ads) nearest-neighbor sites are tested randomly for a CO occupation, if negative the trial ends, if affirmative CO_2(gas) is desorbed and the trial ends; (c2) NO nearest-neighbor sites are tested for empty sites, if none are found the trial ends, otherwise a random number ξ is obtained and, (c21) if $\xi > P$ then the trial ends, (c22) if $\xi \leq P$ then choose one of the vacant nearest-neighbor sites at random, NO is dissociated as N(ads) + O(ads), O(ads) is tested for recombination with a nearest-neighbor CO(ads) as in (c1) and N(ads) is tested to react with nearest-neighbor N or NO, if one is not found the trial ends, if an N is found then reaction step (4) is executed, if an NO is found then the reaction chain follows as in (c1).

(ii) *If the chosen molecule is CO*, then: (a) choose a site at random on the lattice; (b) if the site is occupied, then the trial ends; (c) otherwise CO is adsorbed and nearest-neighbor sites are tested at random for O(ads), if none is found the trial ends, otherwise CO_2(gas) is desorbed and the trial ends.

(iii) *After any adsorption attempt*, either of NO or CO, a desorption step is attempted. A site is chosen at random, if it is not occupied by NO or CO the trial ends, otherwise NO or CO is desorbed with probability D_{NO} or D_{CO}, respectively.

(iv) *After any new vacant site is produced*, its NN sites are tested for an NO, if none is found then the trial ends, otherwise a NO is chosen at random and it is dissociated with probability P. If the dissociation is successful the corresponding reaction chain for each dissociated species is followed, otherwise the trial ends.

It is worth recalling here that if any of the reactant N atoms is adsorbed on a step edge sites then the reaction step in which it is involved, either (4), (5) or (6), is executed with probability I in order to take into account the inhibition effect of those sites.

A Monte Carlo step (MCS) consists of $L \times L$ trials, *i.e.*, in the mean every site on the lattice has been visited for adsorption. For a given value of Y_{CO}, and starting with an initial blank state, stabilization of the process is achieved when the total surface coverage $\theta = \theta_N + \theta_O + \theta_{NO} + \theta_{CO}$ has not changed appreciably over the last 10^4 MCS. In all cases stabilization is achieved before 70×10^4 MCS. In this way a plot of the coverage of each species at steady state, and of the reaction rates R_{N_2}, R_{CO_2}, R_{N_2O} (defined as the number of species produced divided by the number of Monte Carlo trials), *versus* Y_{CO} is obtained. Each steady state result is averaged over 100 independent realizations of the process.

3. Results and discussion

Results for the steady state phase diagram and reaction rate were obtained for lattice sizes $L = 11$, 17, 25 and 57, for values of I ranging from 0 to 1, for $P = 0.5$, 0.7, 0.9, for $D_{CO} = 0.4$ and $D_{NO} = 0.3$ (high temperature) and $D_{NO} = 0$ (low temperature). Table 1 shows the particle size, d, and the proportion of (100) to [(100) + (111)] facets, r, for each lattice size considered. We have chosen a subset of relevant results to be discussed here.

Table 1 Parameters characterizing the size and shape of Pd nanoparticles

L	d/nm	r
11	2.8	0.20
17	4.7	0.22
25	6.9	0.25
57	15.6	0.75

Smallest particle size, $L = 11$

Figs. 2 and 3 show the steady state phase diagram (top) and reaction rates (bottom), for high temperature ($D_{CO} = 0.4$, $D_{NO} = 0.3$) and low temperature ($D_{CO} = 0.4$, $D_{NO} = 0$), respectively, for a dissociation probability $P = 0.7$, and in the extreme case where the reaction of N atoms adsorbed on step edge sites is strongly inhibited, $I = 0$. In the high temperature case, Fig. 2, the surface is poisoned with O and some N at low Y_{CO}. The opening of the reaction window is characterized by a sudden decay in the O coverage and the reactive state persists up to near $Y_{CO} = 1$, where it becomes poisoned mainly with CO and N. The reaction rate shows a sharp increase near $Y_{CO} = 0.5$ and after reaching a maximum decreases slowly towards the high CO concentration region. The behavior for the low temperature case (Fig. 3) is similar except for the following differences which are easily related to the lack of NO desorption: an appreciable amount of undissociated NO contributes to the poisoning of the surface both at low and high CO concentration, the reaction windows shifts appreciably to higher Y_{CO} and the reaction rate is uniformly lower.

The effect of changing the value of I to the other extreme, $I = 1$, not shown here, is merely that of increasing evenly and considerably the reaction rate, due to the fact that the

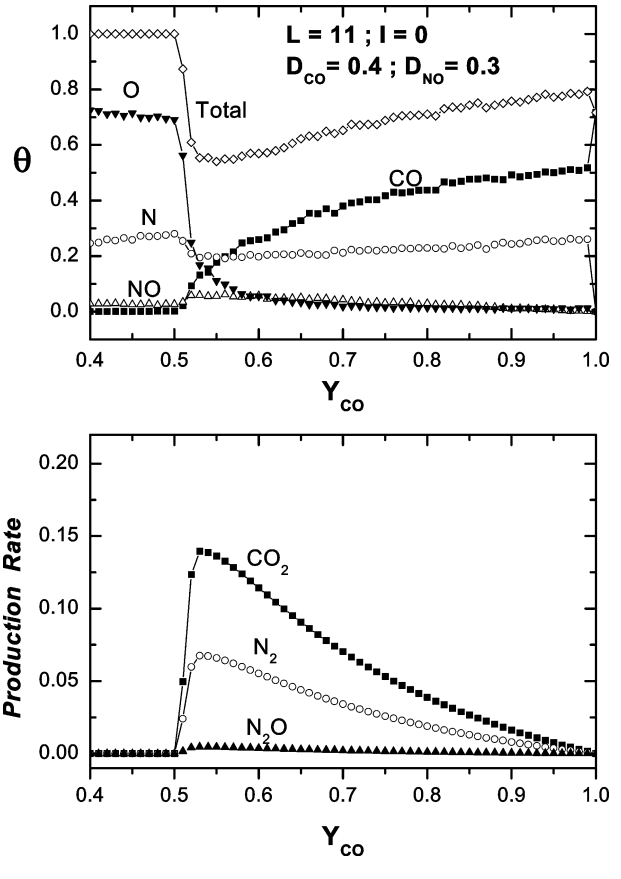

Fig. 2 Steady state coverage, top, and reaction rates, bottom, for Pd nanoparticles of size $L = 11$ with $I = 0$, $D_{NO} = 0.3$ and $D_{CO} = 0.4$ (high temperature).

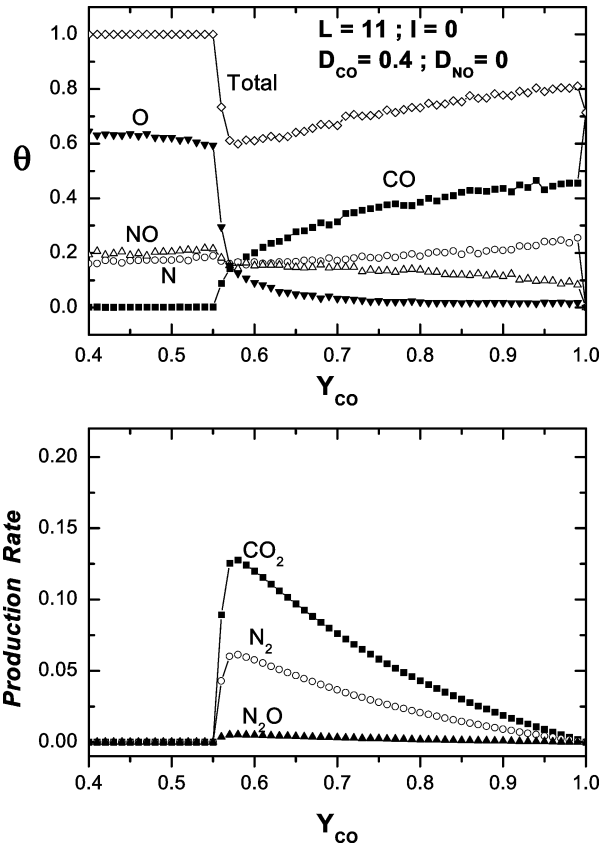

Fig. 3 Steady state coverage, top, and reaction rates, bottom, for Pd nanoparticles of size $L = 11$ with $I = 0$, $D_{NO} = 0$ and $D_{CO} = 0.4$ (low temperature).

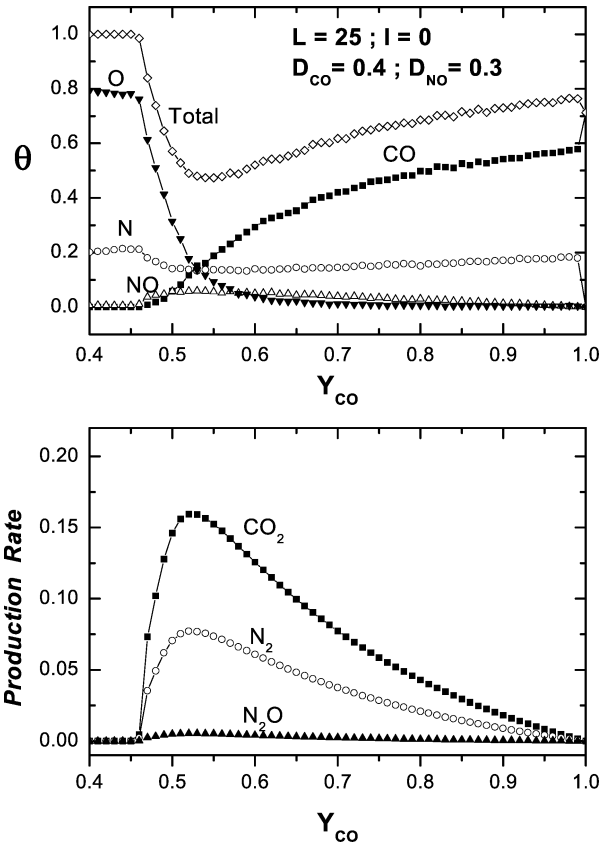

Fig. 4 Steady state coverage, top, and reaction rates, bottom, for Pd nanoparticles of size $L = 25$ with $I = 0$, $D_{NO} = 0.3$ and $D_{CO} = 0.4$ (high temperature).

maximum proportion of edge sites is present for the smallest Pd particle.

Intermediate particle size, $L = 25$

Here we have a larger particle size, but with a similar morphology as compared to the previous case, given that we still have a large proportion of (111) facets. Figs. 4 and 5 show the behavior of the steady state phase diagram and reaction rate, for high and low temperature, respectively, for the same values of parameters as in Figs. 2 and 3. Comparing Fig. 4 with Fig. 2, and Fig. 5 with Fig. 3, we can see that the behavior is quite similar, but now the reaction window extends to lower values of Y_{CO} and the reaction rate is even higher. This, at first sight seems surprising, since the smallest particle ($L = 11$) is the one with the higher proportion of (111) facets, the most active one.[23] However, we must consider here the finite size effects. In fact, in our simulations we do not use periodic boundary conditions, as they should be to simulate nanoscopic scale particles. Therefore all sites at the periphery of active particles have fewer NN sites than those in the bulk, so that NO adsorbed on these sites will have a lower effective dissociation rate. Now, the smallest particles are the ones with the highest proportion of periphery to bulk sites and this overturns the effects of a slightly higher proportion of (111) facets (see Table 1).

Changing the value of I to $I = 1$ does not change this behavior, but we only obtain a uniform increase in the reaction rate, though not so considerable as in the case of the smallest size particle.

Largest particle size, $L = 57$

The largest Pd nanoparticles are characterized by the fact that they present a large proportion of the (100) facet due to a coalescence process occurring during growth of these particles

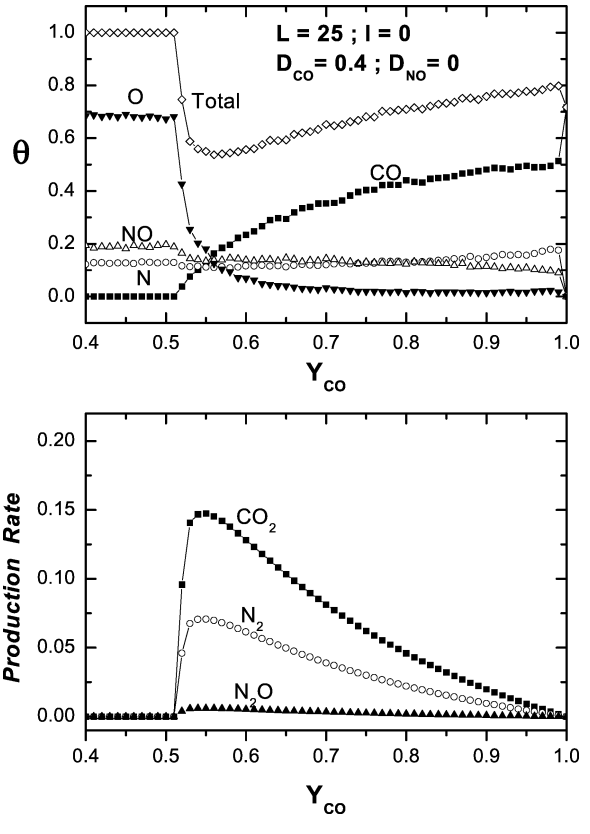

Fig. 5 Steady state coverage, top, and reaction rates, bottom, for Pd nanoparticles of size $L = 25$ with $I = 0$, $D_{NO} = 0$ and $D_{CO} = 0.4$ (low temperature).

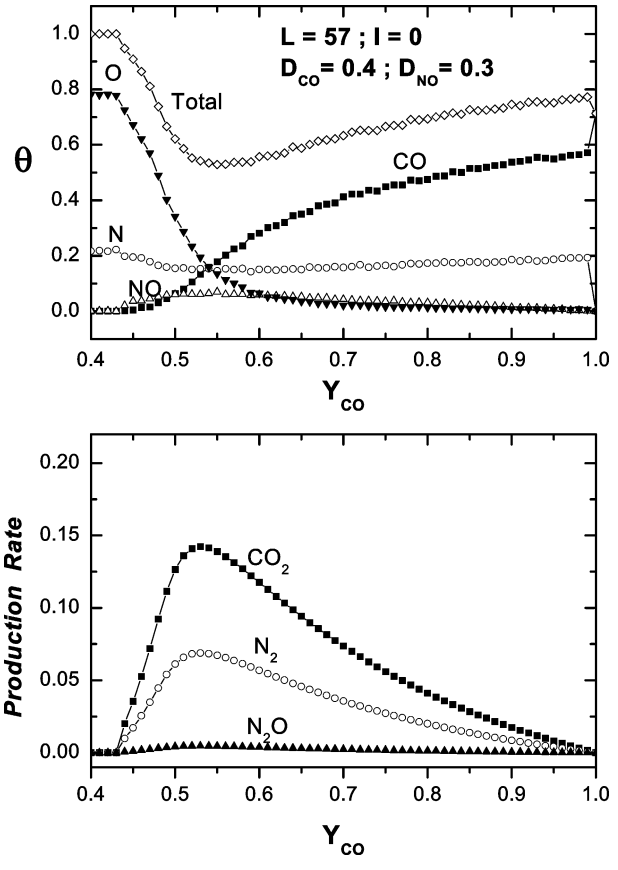

Fig. 6 Steady state coverage, top, and reaction rates, bottom, for Pd nanoparticles of size $L = 57$ with $I = 0$, $D_{NO} = 0.3$ and $D_{CO} = 0.4$ (high temperature).

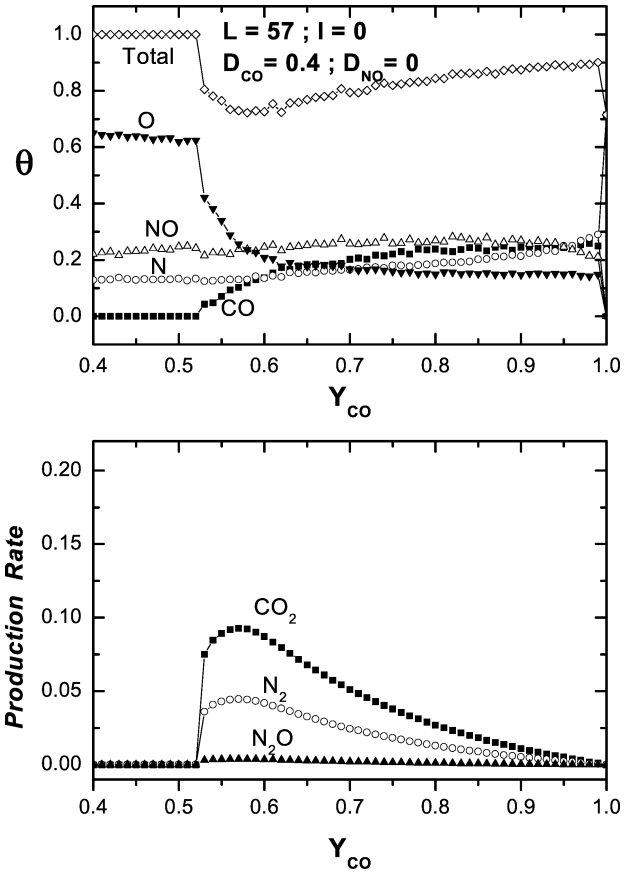

Fig. 7 Steady state coverage, top, and reaction rates, bottom, for Pd nanoparticles of size $L = 57$ with $I = 0$, $D_{NO} = 0$ and $D_{CO} = 0.4$ (low temperature).

for long deposition times.[12] Due to this fact, the desorption of NO becomes extremely important to contribute to the steady state reactivity at low Y_{CO}, since we now have a large proportion of sites with only 4 NN sites, where the effective NO dissociation rate is depressed. The behavior of the kinetics in this case is represented in Figs. 6 and 7, corresponding as before to high and low temperature, respectively, for the same values of the parameters as in Figs. 2 and 3. It can be observed that at high temperature, when NO desorption is active (Fig. 6), the increase of the reaction rate to its maximum is much smoother than for the smallest particle.

By comparing Fig. 6 with Fig. 2, and Fig. 7 with Fig. 3, we see that the largest particles are more active than the smallest ones at high temperature, while the smallest ones are more active than the largest at low temperature. It can also be observed, by comparing with Figs. 4 and 5, that the medium size particles are still the most active ones in any case.

Parameter I, in the case of the largest particles, presents now practically no effect at all, due to the small proportion of edge sites.

4. Comparison with experiments

Experimental reaction rates for the different Pd particle sizes are presented as NO reaction probability, from ref. 12, in Fig. 8, as a function of temperature. This probability was used as a better alternative to the traditional turn-over-number, and was defined as the probability for an NO molecule arriving on a Pd particle to react. Clearly this definition also corresponds to our simulated NO reaction rate.

We can clearly distinguish two temperature regions; say below and above 285 °C. In the low temperature region the smallest particles are more active than the largest ones, while in the high temperature region the relationship is reversed. All over the temperature range, the medium size particles are seen to be the most active ones. These data were obtained at a relative concentration in the direct NO + CO beam of $Y_{CO} \approx 0.5$. However, Pd particles used in the experiments were supported on MgO and it was found that there was a considerable contribution of physisorbed NO and CO diffusing toward the metal particles, in such a way that the data more likely correspond to an average over a wider range of Y_{CO}.

Taking this into account, and for a better comparison with experiments, we have integrated our simulated NO reaction

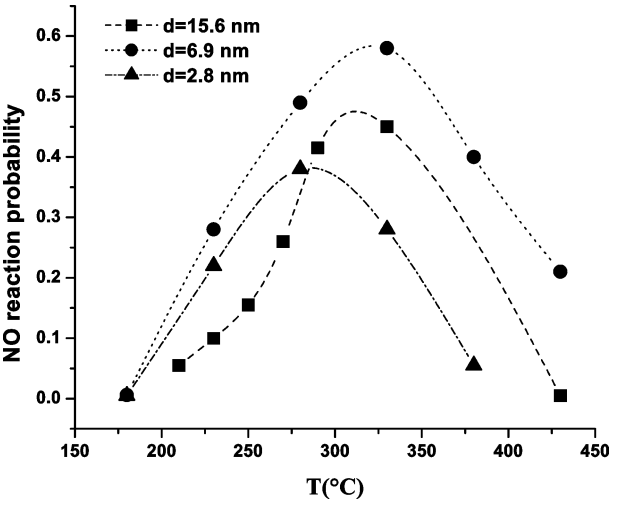

Fig. 8 Experimental data from ref. 12 showing the NO reaction probability as a function of temperature for different particle sizes, d, at $Y_{CO} \approx 0.5$. Notice the different activity–size relationship below and above 285 °C.

rates over Y_{CO}, and have then represented in Fig. 9 the total production of N_2 as a function of the particle size, for high (top) and low (bottom) temperature. Here we can see the same behavior as observed in the experimental data with respect to the relative activity of different particle sizes. We can also see that the effect of step edge sites inhibition, parameter I, which is stronger for smaller sizes as expected, is not enough to overturn the activity–size relationship.

Our simulations provide a very simple explanation of what seemed in ref. 12 the most puzzling result, *i.e.* the fact that the medium size particles were found to be the most active ones. We can now say that this is so because the medium size particles have the right balance between a high ratio of (111)-to-(100) facets and still a not too high proportion of peripheral-to-bulk sites (which is not the case for the smallest size particles). The same kind of finite size effect seems to be responsible for the activity–size relationship between the largest and the smallest particles at high and low temperature. In fact, at low temperature, where desorption of NO is depressed, the largest particle is the less active one because it has a large proportion of the (100) facet. Here the lack of NO desorption causes the effect of the NO dissociation process, which is less effective on (100) facets, to become critical, and this is not counterbalanced enough by the large proportion of peripheral sites in the smallest size particles. When enough NO desorption is present, at high temperature, then the importance of the lower effectiveness of NO desorption on (100) facets becomes relatively small and the effect of the large proportion of peripheral sites in the smallest size particles is the one which prevails, thus overturning the activity–size relationship.

The effect of changing P

Fig. 10 summarises the effects of changing the dissociation probability P to extreme values, such as 0.9 and 0.5, compared to the behavior for $P = 0.7$, for just two extreme values of the step edge sites inhibition parameters, $I = 0$ and $I = 1$. For the high temperature case (top) we see that the activity–size relationship is preserved for $P = 0.5$, while it is overturned for $P = 0.9$. In particular, when P is too large, the activity becomes too small, in fact the smallest, for the largest particle size. This effect can be easily understood, since as explained above NO desorption plays a fundamental role at high temperature to make the largest particle more active than the smallest one. However, when the NO dissociation probability becomes too high there is very little molecular NO on the surface and the effect of NO desorption becomes negligible. Now, from our analysis about the experimentally observed behavior of NO dissociation efficiency in Section 2, we could say that such a high value of P for the largest size particle is quite unlikely. On the other hand, for the case of low temperature (bottom), a high value of $P = 0.9$ does not alter the activity–size relationship, while a low value, $P = 0.5$, makes the reaction window disappear and the activity becomes zero for all particle sizes. Again, due to our discussion in Section 2, a value of 0.5 for the dissociation efficiency is the lowest one observed, and this value includes already the effect of depressing the dissociation process due to the lack of enough vacant sites, therefore the value of P is likely to be appreciably higher than 0.5. In summary, we could say with some confidence that simulation results are still consistent with experimental observations.

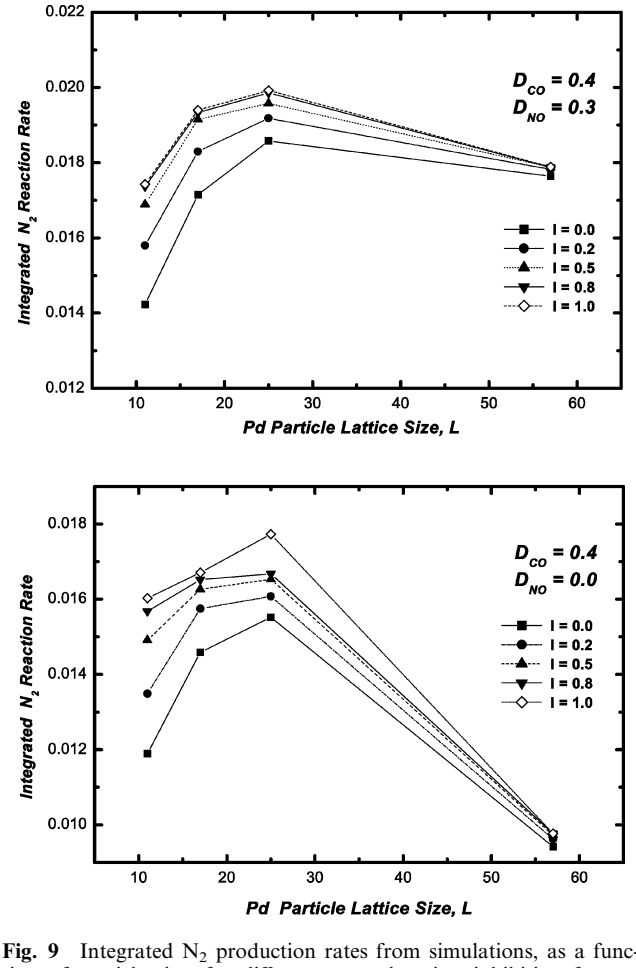

Fig. 9 Integrated N_2 production rates from simulations, as a function of particle size, for different step edge sites inhibition factors, for high (top) and low (bottom) temperature.

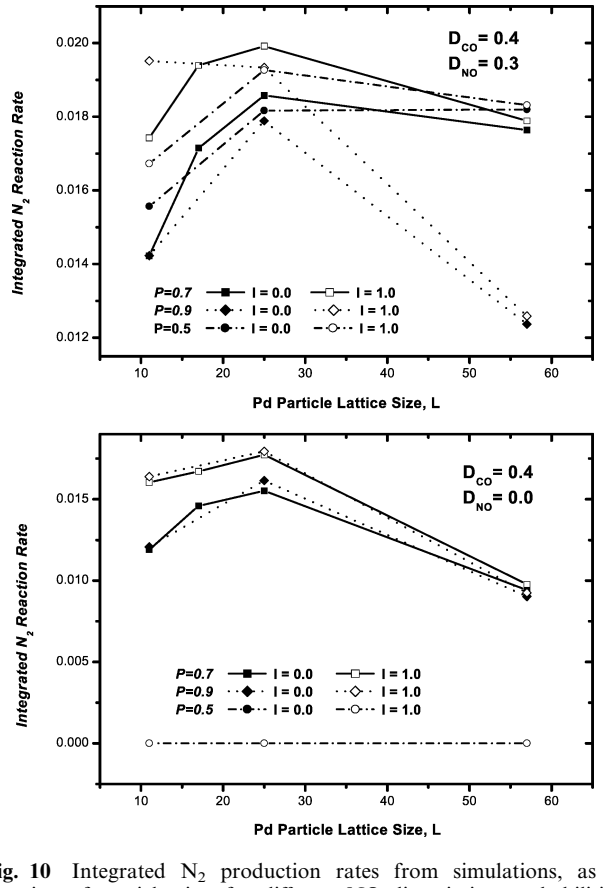

Fig. 10 Integrated N_2 production rates from simulations, as a function of particle size, for different NO dissociation probabilities and step edge sites inhibition factor, for high (top) and low (bottom) temperature.

5. Conclusions

We have studied through Monte Carlo simulations the behavior of the reaction window and reaction rates in the steady state for the NO–CO reaction on Pd nanoparticles of different finite sizes and morphologies, presenting different proportions of (100) and (111) facets. The present study is motivated by the experimental realization of realistic systems for the reduction of NO by CO developed in ref. 12, and the simulation model is developed in such a way as to take into account the main characteristics of the experimental system. The main parameters of the model are the NO dissociation probability, P, the step edge sites inhibition factor I, and the NO and CO desorption probabilities, D_{NO} and D_{CO}, respectively.

Since the activation energy for NO desorption on Pd is higher than that for CO desorption, we studied two limiting cases: the high temperature limit, where both NO and CO desorption are active, and the low temperature limit, where NO desorption is depressed.

Simulation results show that intermediate size particles are the most active over all temperature ranges, while the smallest size particles are the less active at high temperature and the largest size particles are the less active at low temperature, providing simple explanations to this behavior, which are consistent with experimental observations. It is also found that variations in parameters P and I do not change the activity–size relationship and that the NO desorption process and finite size effects are the main factors determining such a relationship.

The model used here, without pretending to establish a general theoretical basis for the analysis of the kind of systems studied, does provide, though through the use of some empirical parameters, a consistent explanation and justification of the set of experimental data observed for the NO–CO reaction on Pd nanoclusters. In this sense, it may also be applied to study the same reaction on other supported metal particles, given that the general behavior does not depend on the nature of the metal but mainly on the fact that supported particles of different sizes will present different proportions of (100) and (111) facets.

Acknowledgements

This research was partially supported by the Consejo Nacional de Investigaciones Científicas y Técnicas (CONICET) of Argentina.

References

1 K. C. Taylor, *Catal. Rev. Sci. Eng.*, 1993, **35**, 457.
2 M. Shelef and G. W. Graham, *Catal. Rev. Sci. Eng.*, 1994, **36**, 433.
3 R. J. Farrauto and R. M. Heck, *Catal. Today*, 2000, **55**, 179.
4 F. Zaera and C. S. Gopinath, *J. Mol. Catal. A*, 2001, **167**, 23.
5 C. S. Gopinath and F. Zaera, *J. Phys. Chem. B*, 2000, **104**, 3194.
6 L. H. Dubois, P. K. Hansma and G. A. Somorjai, *J. Catal.*, 1980, **65**, 318.
7 T. W. Root, L. D. Schmidt and G. B. Fisher, *Surf. Sci.*, 1983, **134**, 30.
8 T. W. Root, L. D. Schmidt and G. B. Fisher, *Surf. Sci.*, 1985, **150**, 173.
9 C. H. F. Peden, D. W. Goodman, D. S. Blair, P. J. Berlowitz, G. B. Fisher and S. H. Oh, *J. Phys. Chem.*, 1988, **92**, 1563.
10 C. Duriez, C. R. Henry and C. Chapon, *Surf. Sci.*, 1991, **253**, 190.
11 L. Piccolo and C. R. Henry, *Appl. Surf. Sci.*, 2000, **162–163**, 670.
12 L. Piccolo and C. R. Henry, *J. Mol. Catal. A*, 2001, **167**, 181.
13 K. Yaldram and M. A. Khan, *J. Catal.*, 1991, **131**, 369.
14 B. J. Brosilow and R. M. Ziff, *J. Catal.*, 1992, **136**, 275.
15 B. Meng, W. H. Weinberg and J. W. Evans, *Phys. Rev. E*, 1993, **48**, 3577.
16 B. Meng, W. H. Weinberg and J. W. Evans, *J. Chem. Phys.*, 1994, **101**, 3234.
17 M. Tammaro and J. W. Evans, *J. Chem. Phys.*, 1998, **108**, 7795.
18 E. V. Albano, *Het. Chem. Rev.*, 1996, **3**, 389.
19 V. P. Zhdanov and B. Kasemo, *Surf. Sci. Rep.*, 1997, **29**, 31.
20 V. Bustos and G. Zgrablich, *Int. J. Mod. Phys.*, 1999, **10**, 1077.
21 F. Zaera, C. S. Gopinath, V. Bustos, R. Uñac and G. Zgrablich, *J. Chem. Phys.*, 2001, **114**, 10 927.
22 S. M. Vesecky, D. R. Rainer and D. W. Goodman, *J. Vac. Sci. Technol. A*, 1996, **14**, 1457 see also B. Hammer, *Faraday Discuss.*, 1998, **110**, 323.
23 D. R. Rainer, S. M. Vesecky, M. Koranne, W. S. Oh and D. W. Goodman, *J. Catal.*, 1997, **167**, 234.
24 L. Piccolo and C. R. Henry, *Surf. Sci.*, 2000, **452**, 198.